JOURNAL OF MATERIALS SCIENCE 30 (1995) 1462–1468

Synthesis and physicochemical properties of cobalt aluminium hydrotalcites

S. KANNAN, S. VELU, V. RAMKUMAR, C.S. SWAMY
Department of Chemistry, Indian Institute of Technology, Madras 600 036, India

Cobalt aluminium hydrotalcites with different compositions were prepared by a coprecipitation method under low supersaturation conditions. The compounds were characterized by X-ray diffraction (XRD), infrared absorption (IR), thermogravimetric analysis (TGA), differential scanning calorimetry (DSC) and BET surface area measurements. XRD and IR studies revealed that all the compounds are single-phase crystallized under a hydrotalcite-like network. Hydrothermal treatments given to the aged sample increased the crystallinity of the samples. TG studies showed two stages of weight loss, the first due to the removal of interlayer water and the second ascribed to the removal of water molecules from the brucite sheet and CO_2 from the interlayer carbonate anion, whose transition temperature depends on the Co/Al atomic ratio. Thermal calcination of these materials results in the formation of high surface area non-stoichiometric spinel phase whose crystallinity increases with increase in the calcination temperature attributed to the sintering of the particles.

1. Introduction

Layered double hydroxides, also known as hydrotalcites, first synthesized by Feitknecht [1] have received considerable attention in recent years owing to their potential application as ion exchangers, adsorbents and, most important, as catalysts [2–9]. They consist of a brucite-like network ($Mg(OH)_2$) wherein the divalent ion is substituted by a trivalent ion whose excess positive charge is compensated by anions occupying the interlayer space. These metal ions occupy the octahedral sites with edge sharing, which constitutes a layer and interlayer network whose structure is efficiently used for molecular sieving and adsorption, similar to zeolites. A recent review by Cavani *et al.* [10] furnishes detailed synthesis and characterization of these materials. These compounds are represented by the general formula $[M(II)_{1-x}M(III)_x(OH)_2]^{x+}\ A^{n-}_{x/n} \cdot mH_2O$, where M(II) and M(III) are divalent and trivalent metal ions, A is the interlayer anion and x can have values $0.15 \leqslant x \leqslant 0.40$.

Thermal calcination of these materials results in the formation of high surface area non-stoichiometric mixed metal oxides which are extensively used in many catalytic transformations, such as steam reforming, methanol synthesis, aldol condensation, N_2O decomposition and polymerization reactions [11–15]. Although a wide variety of divalent metal ions such as nickel, zinc, magnesium, etc, are incorporated into the network, literature available on cobalt-containing hydrotalcites is scarce [16]. The present paper reports the synthesis and characterization of a series of cobalt aluminium hydrotalcites.

2. Experimental procedure

2.1. Sample preparation

The materials are prepared by coprecipitation under low supersaturation conditions [17], wherein a solution of metal nitrates, namely $Co(NO_3)_2 \cdot 6H_2O$ and $Al(NO_3)_3 \cdot 9H_2O$, of appropriate concentrations, is added simultaneously with $NaOH/Na_2CO_3$ (7–8 g/1.5 g) solution at room temperature with vigorous stirring, maintaining the pH between 9 and 10. The addition took 40 min and the final pH was adjusted to 10. The resultant gel was aged at 65 °C for 30 min with vigorous stirring. Part of this solution was subjected to hydrothermal treatment, in a stainless steel autoclave at 110 °C for 2 days under autogenous conditions. The precipitate was filtered, washed with distilled water, and dried in oven at 70 °C overnight.

2.2. Measurements

Elemental analysis of Co^{2+} and Al^{3+} was carried out by inductively coupled plasma emission spectrometry (ICPES) (Model 3410, ARL) by dissolving the compounds in a minimum amount of dilute hydrochloric acid. The X-ray diffraction patterns (XRD) of the samples were taken in a Philips X-ray generator (Model PW1130) using iron-filtered Co$K\alpha$ radiation ($\lambda = 0.17902$ nm) at a scan speed of $3° \text{ min}^{-1}$. Fourier transform–infrared (FT-IR) absorption studies were carried out in the form of KBr pellets in a Perkin–Elmer (Model 1760) in the range 4000–400 cm^{-1}. Thermogravimetric/differential scanning calorimetry (TG/DSC) of these compounds was recorded in a Perkin–Elmer TG/DSC7 in the

0022–2461

temperature range 50–600 °C at a heating rate of 10 °C min^{-1} under a nitrogen atmosphere. The surface area of the samples was measured employing the BET adsorption method in a Carlo–Erba (Model 1800) sorptometer at 77 K. Hereafter, the samples are indicated by their composition followed by the method of preparation, for example, Co–Al2.0:1-A or H indicates the Co/Al atomic ratio is 2.0 prepared under ageing (A) or hydrothermal (H) treatments, respectively.

3. Results and discussion

The X-ray diffraction patterns of aged and hydrothermally treated samples are shown in Fig. 1. All compounds crystallized in the single phase with hydrotalcite structure, showing sharp and symmetrical reflections for (0 0 3), (0 0 6), (1 1 0) and (1 1 3) planes, and broad and asymmetrical peaks for (1 0 2), (1 0 5) and (1 0 8) planes which are characteristic of these materials possessing a layered structure [18]. The lattice parameters were calculated by indexing the peaks under a hexagonal crystal system by least squares fitting for the peaks whose $2\theta \geqslant 45°$ and are summarized in Table I. It can be clearly inferred that as the Co/Al atomic ratio increases, the lattice parameters a and c increase with the net increase in the unit cell volume.

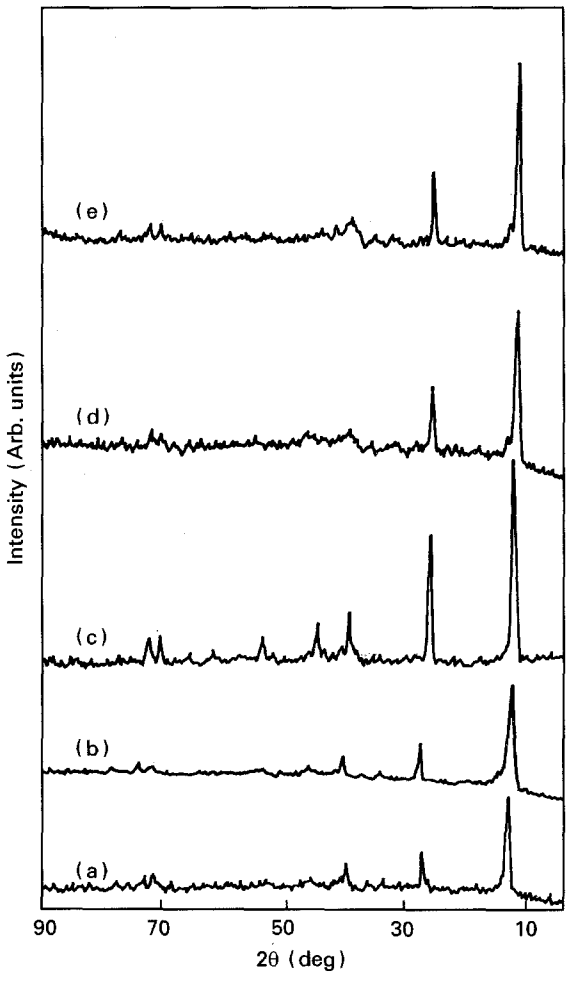

Figure 1 X-ray diffraction patterns of (a) Co–Al2:1-A, (b) Co–Al2:1-A*, (c) Co–Al2:1-H, (d) Co–Al3:1-A, and (e) Co–Al3:1-H.

TABLE I The cell parameters and surface area of the samples synthesized

Sample	M^{2+}/M^{3+} (atomic ratio)	a (nm)	c (nm)	V (10^{-3} nm^3)	Surface area ($m^2 g^{-1}$)
Co–Al2.0:1-A	2.0	0.3052	2.2144	178.6	63.6
Co–Al2.6:1-A	2.6	0.3055	2.3057	186.4	57.3
Co–Al3.0:1-A	3.0	0.3059	2.3578	191.1	35.0
Co–Al2.0:1-H	2.0	0.3064	2.2707	184.6	28.7
Co–Al2.6:1-H	2.6	0.3065	2.3193	188.7	–
Co–Al3.0:1-H	3.0	0.3075	2.2849	187.1	18.9

TABLE II Particle sizes of the aged and hydrothermally treated samples by X-ray line broadening

Compound	2θ (deg)	hkl	β (deg)	t (nm)	Average t (nm)[a]
Co–Al2.0:1-A	25.967	0 0 6	0.600	15.62	15.6
	73.150	1 1 3	0.800	14.20	
Co–Al2.0:1-H	27.620	0 0 6	0.350	26.27	24.5
	73.155	1 1 3	0.450	25.30	
Co–Al2.6:1-A	27.657	0 0 6	0.500	22.50	23.7
	73.187	1 1 3	0.400	23.00	
Co–Al2.6:1-H	27.635	0 0 6	0.325	28.92	30.0
	73.187	1 1 3	0.375	30.32	
Co–Al3.0:1-A	27.902	0 0 6	0.425	22.13	20.9
	73.480	1 1 3	0.550	20.71	
Co–Al3.0:1-H	13.875	0 0 3	0.425	21.64	22.0
	73.102	1 1 3	0.525	21.64	

[a] Average particle size is calculated using (0 0 3), (0 0 6), (1 1 0) and (1 1 3) planes.

The increase in the lattice parameter a can be attributed to the higher ionic radius of Co^{2+} (0.074 nm) with respect to Al^{3+} (0.050 nm) [19], and the increase in the c parameter is due to less electrostatic interaction prevalent between layer and interlayer. To ensure whether the crystallization is complete at 30 min, the aged sample Co–Al2.0:1 was subjected to further ageing at 65 °C/24 h without stirring the solution. The XRD pattern of this sample (Co-Al2.0:1-A*) showed no change in the crystallinity (Fig. 1) indicating that the crystallization is complete at 30 min.

Hydrothermal treatments were performed on these samples in an attempt to study how the textural properties of the materials becomes modified. As indicated in Fig. 1, this treatment increases the crystallinity of the material as evinced from the sharpness and intensity of the (0 0 3), (0 0 6) and (1 1 0) reflections. This can be attributed to the increases in the crystallite size, which can be confirmed by measuring the particle sizes of the materials. The particle sizes of these materials were calculated employing the X-ray line-broadening technique using the Debye–Scherrer equation, $t = 0.9\,\lambda/\beta\cos\theta$, where t is the particle thickness, λ is the wavelength of the radiation used, β is full width at half maximum (rad) and θ is the Bragg diffraction angle [20], and the values are given in Table II. It is clearly evident from this table that the particle size of the hydrothermally treated materials is larger than the aged materials. This result is also substantiated by surface area measurements, which showed a dramatic loss in the surface area for the

hydrothermally treated samples (Table I). The lattice parameter a for the hydrothermally treated samples given in Table I is high in comparison with the aged sample, which could be due to the better ordering of the brucite-like sheet for the former samples. However, for Co–Al3.0:1, there is no marked increase in the crystallinity, as evinced from XRD and particle-size measurements. A weak peak observed around $2\theta = 17°$ for Co–Al2.6:1 and Co–Al3.0:1, which can arise due to the disorderliness in the interlayer, is completely absent or reduced in its intensity for their corresponding hydrothermally treated samples indicating the enhancement of ordering.

FT–IR absorption spectra of these compounds, given in Fig. 2, showed prominent bands around 3400, 1640 and 1370 cm^{-1} attributed to OH stretching, OH bending, and asymmetrical stretching (ν_3) of carbonate, respectively. The low value of ν_{OH} in comparison with free hydroxide ($> 3650\ cm^{-1}$) indicates that all OH groups are hydrogen bonded. A weak absorption band around $3050\ cm^{-1}$ is observed and is due to water molecules hydrogen-bonded to the carbonate ion present in the interlayer [21]. Bands ν_2 (out-of-plane deformation) and ν_4 (in-plane bending) of carbonate are observed around 870 and $680\ cm^{-1}$, respectively, for all these samples. Differences noticed for all bands between the observed vibrations of carbonate and free carbonate, indicate even perturbation of the anion in the interlayer space. The other bands observed between 800 and $400\ cm^{-1}$ are assigned to lattice vibrations such as Co–Al–O stretching and bending and M–O stretching [22].

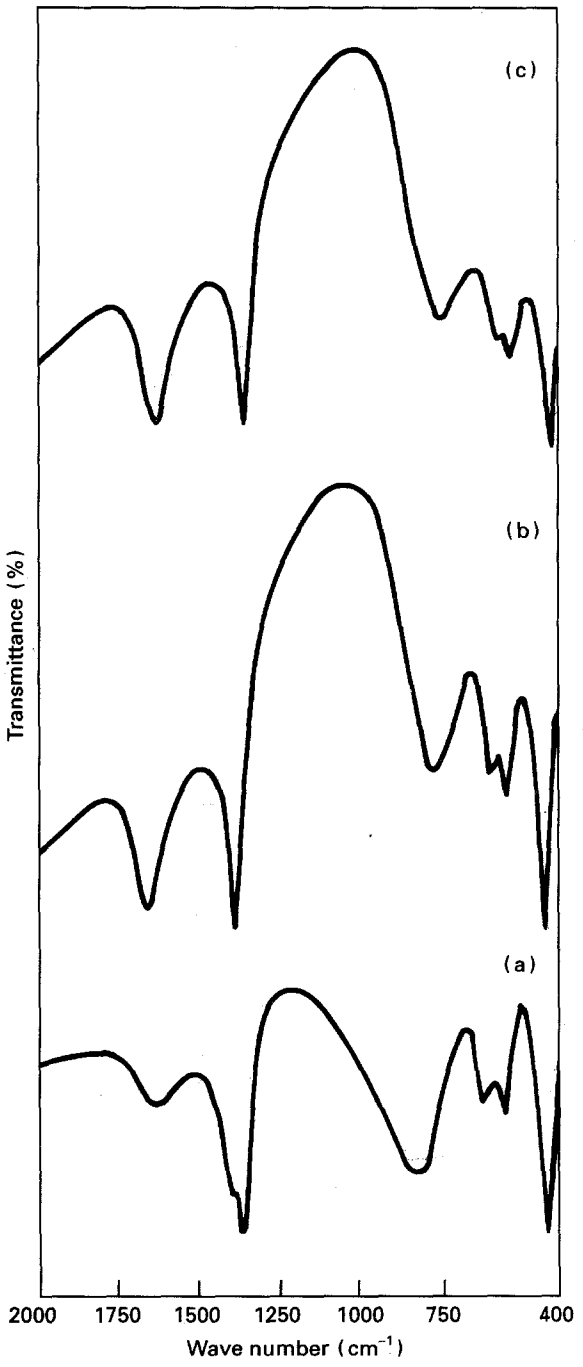

Figure 2 FT–IR spectra of (a) Co–Al2:1-A, (b) Co–Al2.6:1-A and (c) Co–Al3:1-A.

For the sample Co–Al2.0:1-A, the ν_3 mode of carbonate showed splitting at 1385 and $1360\ cm^{-1}$. This could be due to the lower symmetry of carbonate present in the interlayer. For a symmetrical carbonate present in the interlayer, it should be present parallel to the interlayer sheet with D_{3h} symmetry. Owing to its interaction with OH species present in the brucite sheet and H_2O molecules in the interlayer, the symmetry becomes distorted to C_{2v} which causes splitting in the ν_3 mode [21]. This can also cause activation in the ν_1 mode (symmetrical stretching) present around $1030\ cm^{-1}$, which is inactive when the carbonate is present in a symmetrical environment. However, surprisingly, no such band was observed for our samples. Hydrothermal treatment given to this sample showed a sharp single band for ν_3 indicating that this treatment enhances the ordering in the interlayer space to regain its D_{3h} symmetry. For the other two samples, the ν_3 of the aged samples is itself sharp and a single band indicating that the samples are well ordered. This result can be substantiated by X-ray results which showed that the change in the intensity and sharpness of the peaks are more drastic for Co–Al2.0:1-A than for Co–Al3.0:1 upon hydrothermal treatment. However, no shift was noticed in the band position upon hydrothermal treatment.

A closer look at the ν_{OH} and ν_3 values of carbonate for the aged samples indicates that as the Co/Al atomic ratio increases, both the vibrations are shifted to higher wave numbers. This can be attributed on the basis of electrostatic interaction between the layer and the interlayer with a consequent effect on the hydrogen bonding between hydroxyl group and carbonate. As the atomic ratio increases, the interaction decreases with the net effect in the shift to higher wave numbers. This can also be compared with X-ray results which shows that the lattice parameter c increases with increase in the Co/Al atomic ratio, consequently lowering the interaction.

For all the aged samples, ν_{OH} is broad and asymmetrical in nature. However on hydrothermal treatment, it becomes narrow and symmetrical, indicating more orderliness for the hydrothermally treated sample. The band positions and FWHM for all the samples are given in Fig. 3. The ν_{OH} band positions are not altered under the hydrothermal treatment, similar to ν_3 of carbonate, which is in contrast to the

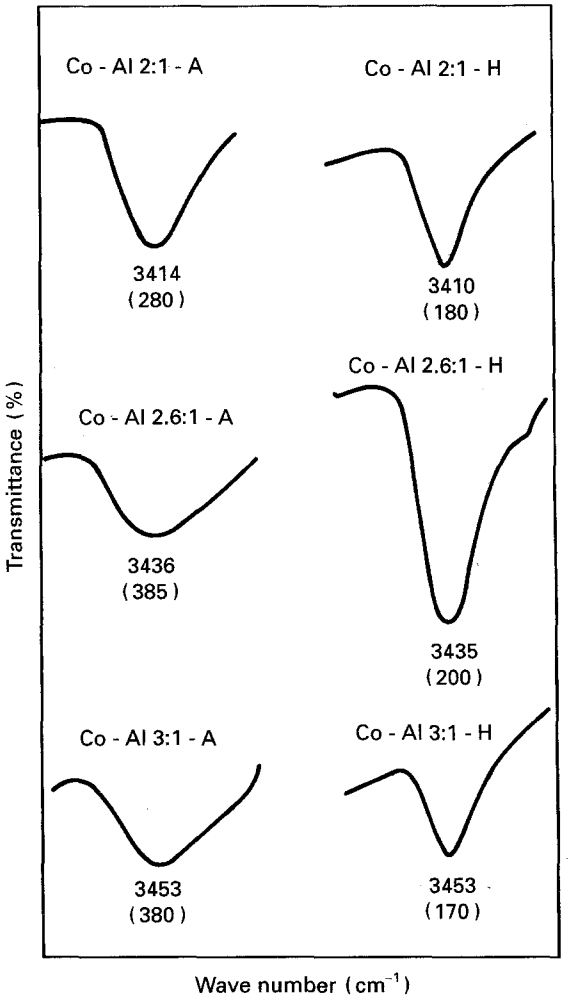

Figure 3 Hydroxyl stretching vibrations of hydrotalcite-like compounds. Values in parentheses are FWHM in cm^{-1}.

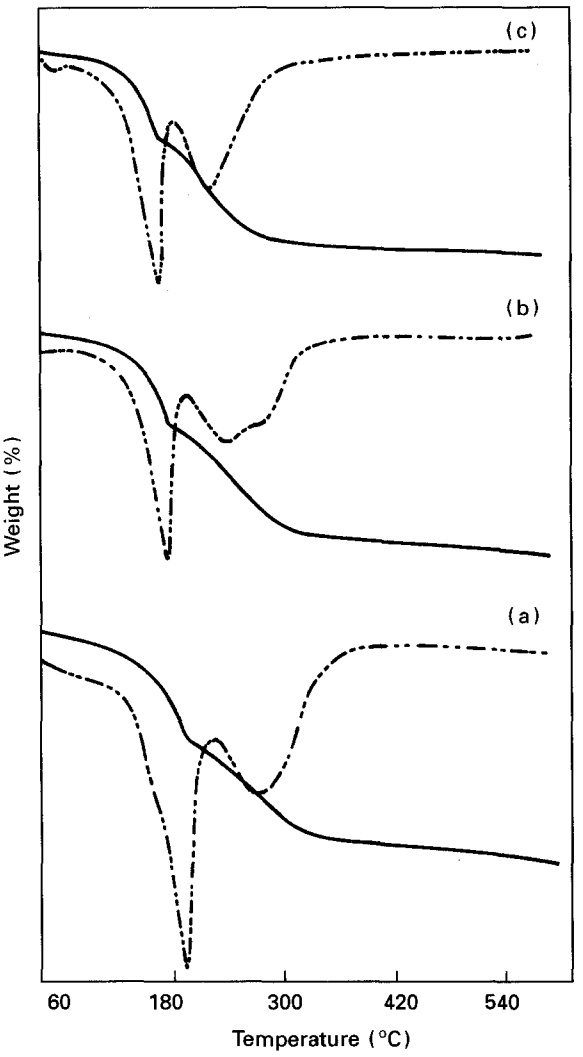

Figure 4 (—) TG and (-·-·) DTG traces for hydrotalcites aged at 65 °C/30 min; (a) Co–Al2:1-A, (b) Co–Al2.6:1-A, (c) Co–Al3:1-A.

result observed by Labajos *et al.* [21] for Mg–Al–CO_3–HT. This is due to the more severe conditions of the treatment employed by them.

Fig. 4 shows the TG and its differential curve for the samples synthesized by ageing. All the compounds showed two stages of weight loss. The first weight loss occurs below 200 °C and is attributed to the removal of interlayer water molecules. The second weight loss, occurring in the temperature range 250–350 °C, is associated with the removal of water from the brucite sheet and CO_2 from the interlayer carbonate anion with the destruction of the layered structure [4]. The corresponding peak appears generally broad because the two processes take place simultaneously. It has been reported in the literature [23] that initially CO_2 is lost, followed by the loss of water molecules in the brucite sheet. Only for the sample Co–Al2.6:1-A, the second stage split into two, corresponding to the loss of CO_2 followed by H_2O.

Table III gives the net weight loss and transition temperature of all the aged samples. It is clearly seen from the table that as the Co/Al ratio decreases, the transition temperatures T_1 and T_2 (for the corresponding weight loss) increases. On substitution of Al^{3+} by Co^{2+}, the positive charge density of the layer increases, which increases the electrostatic interaction. The net weight loss studied in the temperature range

TABLE III TG transition temperature and net weight loss for the aged samples

Compound	TG transition temperature (°C)		Weight loss for first transition (%)	Net weight loss (%)
	T_1	T_2		
Co–Al2.0:1-A	193.3	274.0	14.5	33.4
Co–Al2.6:1-A	184.7	253.4 289.5	13.2	32.4
Co–Al3.0:1-A	178.7	235.4	12.8	29.8

increases with increase in the Al^{3+} content, because more carbonate and water molecules are required for charge compensation.

Differential scanning calorimetry results substantiated the TG results, showing two endothermic peaks for the corresponding two weight losses (Fig. 5). The DSC transition temperature, although higher than TG transition temperature, followed the same trend, i.e. the transition temperature decreases with increase in the Co/Al atomic ratio. Comparison of the DSC curves of aged and hydrothermally treated samples showed an interesting feature in that the DSC curves were more intense and sharper for the hydrothermally treated samples, which is indicative of the higher

crystallinity [24]. No new peaks were found in the DSC of the hydrothermally treated sample, indicating that no new phase is formed and only the hydrotalcite phase is present. The activation energies for the decomposition processes were calculated using Kinetics software employing the Arrhenius equation, and are shown in Table IV.

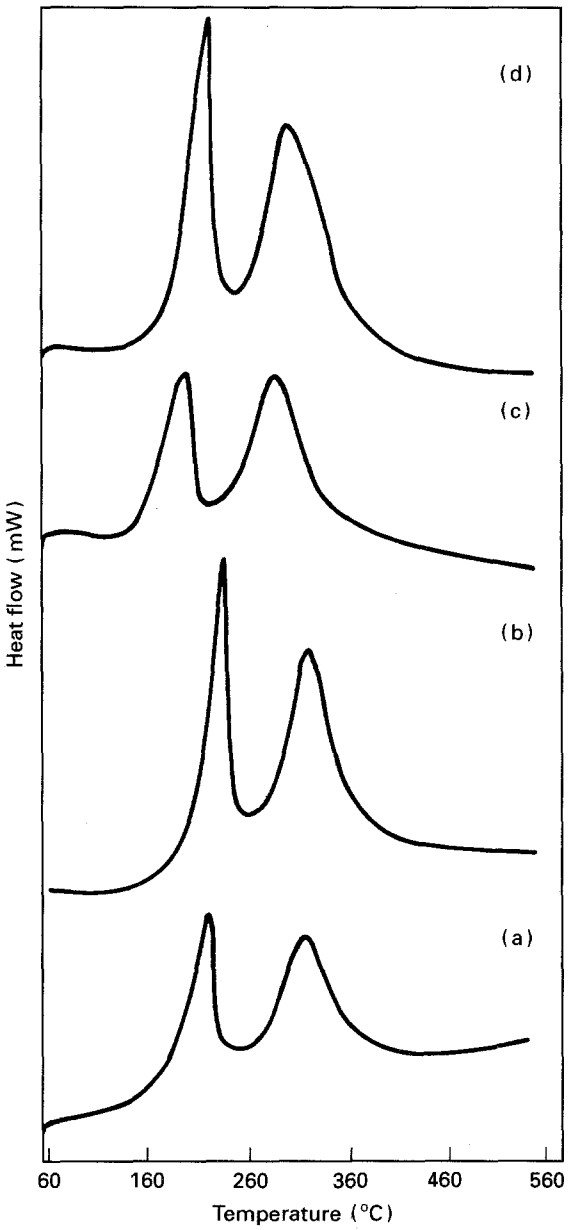

Figure 5 DSC patterns of hydrotalcites: (a) Co–Al2:1-A, (b) Co–Al2:1-H, (c) Co–Al3:1-A, (d) Co–Al3:1-H.

Thermal calcination of the materials has been carried out in order to obtain a better insight into the nature of the thermally decomposed materials. Generally, it leads to the formation of mixed metal oxides of high surface area. In the case of Ni–Al–CO_3–HT [25] and Mg–Al–CO_3–HT [23], thermal calcination results in the formation of corresponding metal oxides, namely NiO and MgO, but at very high temperatures (> 800 °C), spinel formation is encountered. In the case of Co–Al–CO_3–HT, thermal calcination leads to the non-stoichiometric spinel phase even at 200 °C.

Fig. 6 shows the variation of X-ray diffraction pattern of Co–Al2.6:1-A with calcination temperature, holding at each temperature for 1 h. It shows that at

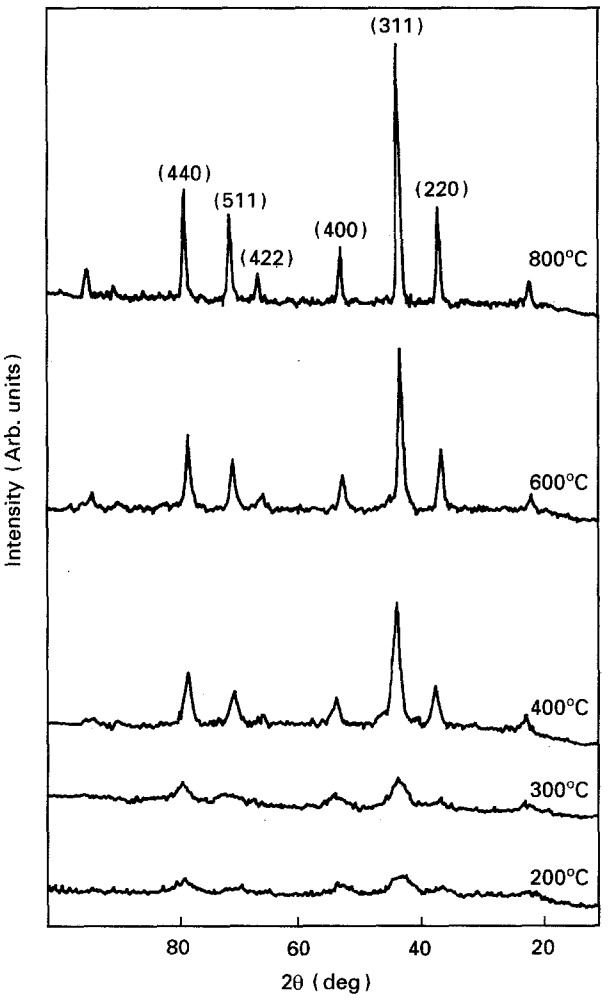

Figure 6 XRD pattern of Co–Al2.6:1-A calcined at different temperatures.

TABLE IV Thermochemical data derived from DSC for the aged and hydrothermally treated samples

Compound	DSC transition temperature (°C)		H_1 (Jg^{-1})	H_2 (Jg^{-1})	E_{a1} ($kJmol^{-1}$)	E_{a2} ($kJmol^{-1}$)
	T_1	T_2				
Co–Al2.0:1-A	227.3	313.2	360	562	134.4	186.5
Co–Al2.0:1-H	232.0	316.3	680	901	205.0	211.0
Co–Al2.6:1-A	220.3	307.7	430	664	153.5	182.9
Co–Al2.6:1-H	217.9	307.7	390	705	176.0	174.7
Co–Al3.0:1-A	197.6	285.9	242	422	120.2	148.6
Co–Al3.0:1-H	215.6	297.6	313	582	159.6	131.0

200 °C, the hydrotalcite-like network collapses and forms a spinel phase with broad peaks. Increase in the calcination temperature increases the crystallinity of the spinel phase, as indicated by the increase in the sharpness and intensity of the XRD peaks. Fig. 7 shows the XRD pattern of all aged samples calcined at 400 °C for 24 h. All the samples gave the spinel phase on calcination. The lattice parameter *a* calculated for this phase is given in Table V. It can be clearly seen that these values are much lower than those of pure $CoAl_2O_4$(0.8105 nm) indicating the presence of Co^{3+} in the spinel which could be obtained by the oxidation of Co^{2+} during calcination, thereby resulting in Co–Al solid solution [26]. The decrease in lattice parameter *a* with increase in Co/Al atomic ratio may be due to the increase in the amount of Co^{3+} in the spinel phase.

These X-ray results were substantiated by surface area measurements, for the samples calcined at different temperatures for 1 h. For all the compounds an increase in the surface area was observed up to 200 °C (Fig. 8) which is explained by the increase in the porosity of the material due to the loss of CO_2 and H_2O. The exiting steam and CO_2 escape through the pores in the crystal surface which appear as small craters in the TEM, and is responsible for the initial increase in the surface area [27]. The collapse of the structure at 200 °C is evinced from the XRD results. Further increase in the calcination temperature leads to a drop in the surface area, which could be attributed to the sintering of the mixed metal oxide particles. This is confirmed by the increase in the crystallinity of the materials, as evinced from XRD. The fall in the surface area is greater for Co–Al hydrotalcite-like materials in comparison with Ni–Al hydrotalcites [28], owing to the stronger interaction between NiO and Al_2O_3, thereby preventing the sintering of the metal oxide particles.

4. Conclusion

XRD results showed that all the compounds crystallize in the hydrotalcite phase whose lattice parameters increase with increase in the Co/Al atomic ratio. IR spectra of these materials showed a pattern similar to natural mineral hydrotalcite with ν_{OH} and ν_3 of carbonate band position dependent on Co/Al atomic ratio. As the Co/Al atomic ratio increases, both the vibrations are shifted to higher wave numbers. Hydrothermally treated samples showed a similar pattern with the change in the band widths of ν_{OH}, attributed to enhanced ordering. TG data showed two stages of weight loss, the first due to the removal of

TABLE V The lattice parameters and the surface area of the aged samples calcined at 400 °C for 24 h

Compound	*a* (nm)	Surface area ($m^2 g^{-1}$)
Co–Al2.0:1-A	0.8061	113.6
Co–Al2.6:1-A	0.8041	136.1
Co–Al3.0:1-A	0.8030	132.0
$CoAl_2O_4$	0.8105	–

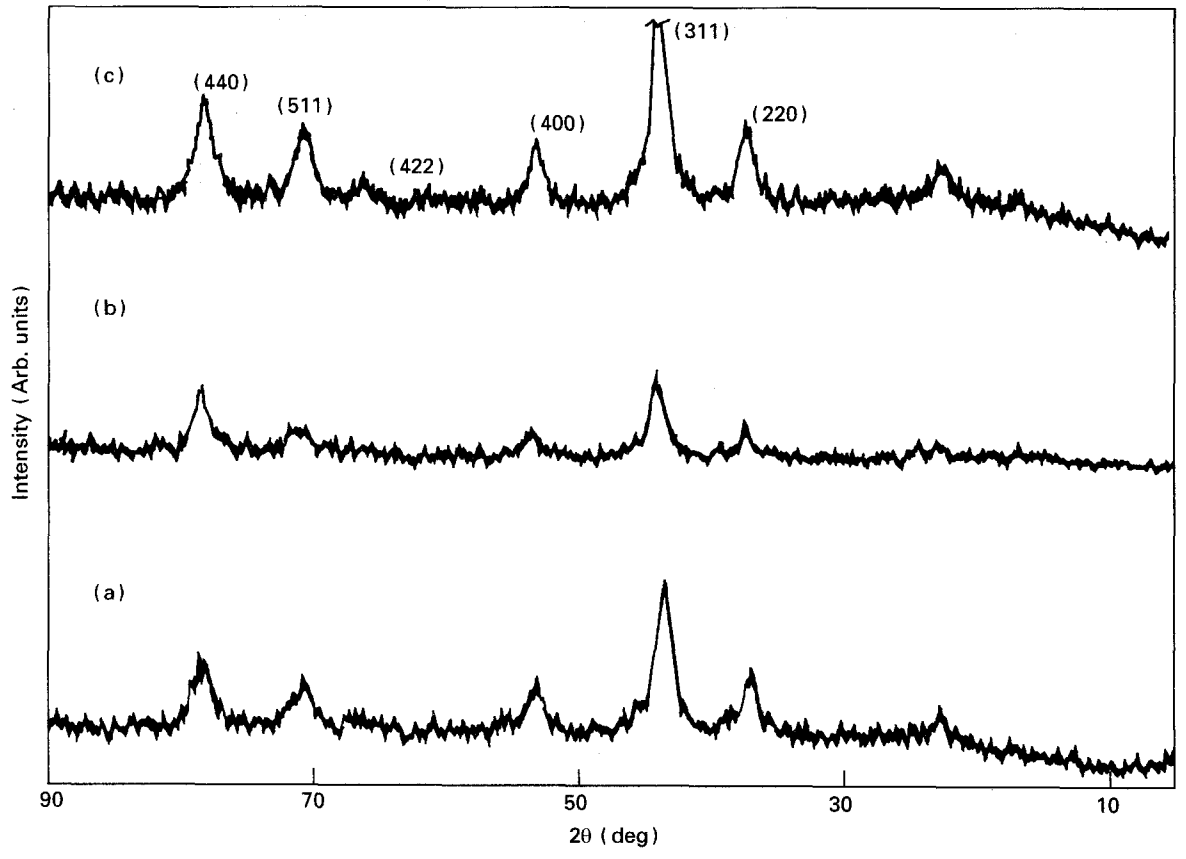

Figure 7 X-ray diffraction patterns of hydrotalcites calcined at 400 °C/24 h: (a) Co–Al2:1-A, (b) Co–Al2.6:1-A, (c) Co–Al3:1-A.

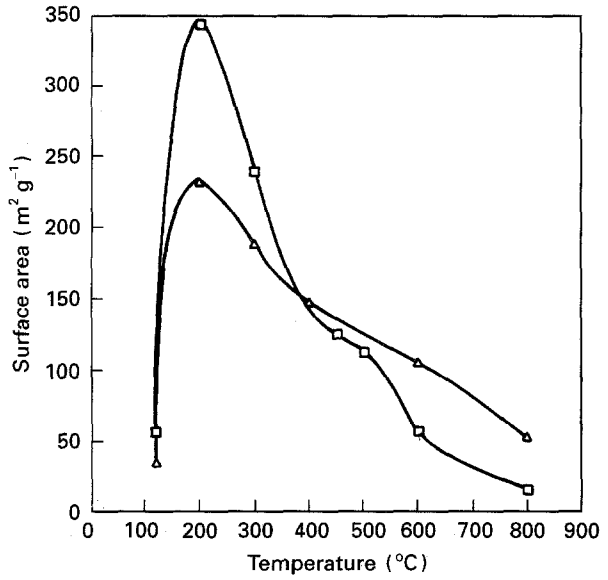

Figure 8 Variation of surface area with calcination temperature, for (□) Co–Al2.6:1-A and (△) Co–Al3.0:1-A.

interlayer water, and the second ascribed to the removal of H_2O from the brucite sheet and CO_2 from the interlayer carbonate anion whose transition temperature and net weight loss increases with decrease in Co/Al atomic ratio. Thermal calcination of these materials resulted in the formation of a spinel-type phase, whose crystallinity increases with increase in the calcination temperature, with subsequent decrease in the surface area attributed to sintering of the particles.

Acknowledgements

Two of the authors (S.K. and S.V.) thank Miss Dorothy for surface area measurements, and the Indian Institute of Technology for financial assistance.

References

1. W. FEITKNECHT, *Helv. Chem. Acta* **25** (1942) 131.
2. R. ALLMANN, *Acta Cystallogr.* **24** (1968) 972.
3. H. F. W. TAYLOR, *Mineral. Mag.* **39** (1973) 377.
4. S. MIYATA, *Clays Clay Miner.* **23** (1975) 369.
5. W. T. REICHLE, *Solid State Ionics* **22** (1986) 135.
6. K. A. CORRADO, A. KOSTAPAPAS and S. L. SUIB, *ibid.* **26** (1988) 77.
7. H. C. B. HANSEN and R. M. TAYLOR, *Clay Miner.* **25** (1990) 161.
8. T. J. PINNAVAIA, NATO ASI Ser., Ser. C, Zeolite Microporous Solids: Synthesis, structure and reactivity (1992) p. 91.
9. S. KANNAN and C. S. SWAMY, *J. Mater. Sci. Lett.* **11** (1992) 1585.
10. F. CAVANI, F. TRIFIRO and A. VACCARI, *Catal. Today* **11** (1991) 173.
11. E. C. KRUISSINK, L. L. VAN REIJEN and J. R. H. ROSS, *J. Chem. Soc. Farad. Trans. I* **77** (1981) 665.
12. O. CLAUSE, M. GAZZANO, F. TRIFIRO, A. VACCARI and L. ZOTORSKI, *Appl. Catal.* **73** (1991) 217.
13. W. T. REICHLE, *J. Catal.* **94** (1985) 547.
14. S. KANNAN and C. S. SWAMY, *Appl. Catal. B*, **3** (1994) 109.
15. D. E. LAYLOCK, R. L. COLLACOAT, D. A. SKELTON and M. F. TCHIR, *J. Catal.* **130** (1991) 354.
16. T. SATO, H. OKUYAMA, T. ENDO and M. SHIMADA, *React. Solids* **8** (1990) 63.
17. S. KANNAN and C. S. SWAMY, in "INDO-US workshop on Perspectives in New Materials", New Delhi, India, 23–24 March 1992, abstract p. 75.
18. S. MIYATA, *Clays Clay Miner.* **31** (1983) 305.
19. R. D. SHANNON and C. T. PREWITT, *Acta Crystallogr.* **B25** (1969) 925.
20. B. D. CULLITY, in "Elements of X-ray Diffraction" (Addison-Wesley, Reading, MA, 1987) p. 284.
21. F. M. LABAJAS, V. RIVES and M. A. ULIBARRI, *J. Mater. Sci.* **27** (1992) 1546.
22. M. J. HERNANDEZ-MORENO, M. A. ULIBARRI, J. L. RENDON and C. J. SERNA, *Phys. Chem. Miner.* **12** (1985) 34.
23. L. PESIC, S. SALIPUROVIC, V. MARKOVIC, D. VUCELIC, W. KAGUNYA and W. JONES, *J. Mater. Chem.* **2** (1992) 1069.
24. A. J. MARCHI, J. I. DI COSIMO and C. R. APESTIGUIA, in "Proceedings of the 9th International Congress on Catalysis", Vol. 2, Chemical Institute of Canada, Ottawa, edited by M. J. Phillips and M. Ternan (1988) p. 529.
25. M. J. HERNANDEZ, M. A. ULIBARRI, J. L. RENDON and C. J. SERNA, *Thermochim. Acta* **81** (1984) 187.
26. P. GARCIA CASADO and I. RASINES, *J. Solid State Chem.* **52** (1984) 187.
27. W. T. REICHLE, S. Y. KANG and D. S. EVERHARDT, *J. Catal.* **101** (1986) 352.
28. E. C. KRUISSINK, L. E. ALZAMORA, S. ORR, E. B. M. DOESBURG, L. L. VAN REIJEN, J. R. H. ROSS and G. VAN VEEN, in "Preparation of Catalysts II", Studies in Surface Science Catalysis, Vol. 3, edited by B. Delmon, P. Grange, P. A. Jacobs and G. Poncelet (Elsevier, Amsterdam, 1979) p. 143.

Received 15 December 1993
and accepted 13 October 1994